# Polymer/Carbon Nanotube Composite Film Formation: A Fluorescence Study

**Önder Yargı,[1] Şaziye Uğur,[2] Önder Pekcan[3]**
[1]*Yildiz Technical University, Department of Physics, Esenler, 34210 Istanbul, Turkey*

[2]*Istanbul Technical University, Department of Physics, Maslak, 34469, Istanbul, Turkey*

[3]*Kadir Has University, Faculty of Arts and Science, Cibali, 34320, Istanbul, Turkey*

**In this study, the effect of multi-walled Carbon nanotube (MWNT) on film formation behavior of Polystrene (PS) latex film was investigated by using steady state fluorescence technique. Films were prepared by mixing of pyrene (P)-labeled PS latex with different amounts of MWNTs varying in the range between 0 and 20 wt%. After drying, MWNT containing films were separately annealed above glass transition temperature ($T_g$) of PS ranging from 100 to 270°C for 10 min. In order to monitor film formation behavior of PS/MWNT composites, Scattered light ($I_s$) and fluorescence intensities ($I_P$) from P were measured after each annealing step to monitor the stages of film formation. At 0–20 wt% range of MWNT content films, minimum film formation ($T_o$), void closure ($T_v$), and healing, ($T_h$) temperatures were determined. Void closure and interdiffusion stages were modeled and related activation energies were determined. It was observed that while void closure activation energies increased, backbone activation energies decreased as the percent of MWNT is increased in the composite films. POLYM. COMPOS., 35:817–826, 2014.** © 2013 Society of Plastics Engineers

## INTRODUCTION

As a result of worldwide efforts by theorist and experimentalists, a very good understanding of the mechanisms of latex film formation has been achieved [1]. Traditionally, the film formation process of polymer latex is considered in terms of three sequential steps: (i) water evaporation and subsequent packing of polymer particles (ii) deformation of the particles and close contact between the particles if their $T_g$ is less than or close to the drying temperature (soft or low $T_g$ latex). Latex with a $T_g$ above the drying temperature (hard or high $T_g$ latex) stays undeformed at this stage. In the annealing of hard latex system, deformation of particles first leads to void closure [2, 3] and then after the voids disappear, diffusion across particle–particle boundaries starts, i.e., the mechanical properties of hard latex films evolve during annealing, after all solvent has evaporated and all voids have disappeared. (iii) Coalescence of the deformed particles to form a homogeneous film [3] where macromolecules belonging to different particles mix by interdiffusion [5, 6].

This understanding of latex film formation can now be exploited to underpin the processing of new types of coatings and adhives. The blending of latex particles and inorganic nanoparticles provides a facile means of ensuring dispersion at the nanometer scale in composite coatings.

Ever since the first scientific report of carbon nanotubes (CNTs) in 1991, these materials have attracted enormous interest owing to their potential applications in field-emission devices, electronics, fibers, composites, sensors, detectors, capacitors, hydrogen storage media, and fuel cells, among others [7]. As of January of 2004, 152 patents relating to nanotube applications had been issued, and another 274 were pending. Recent work by numerous groups has demonstrated how nanocomposites of polymers and CNTs offer the advantages of polymers, such as optical clarity, viscoelasticity and good barrier properties, combined with the strength [8] and the high thermal and electrical conductivity [9] of CNTs. Seven patents have already been issued for CNT nanocomposites and fibers. Four of the most common processing routes for this class of nanocomposites are (1) in situ polymerization [10], (2) melt processing and extrusion [11], (3) casting from a common solvent [12], and (4) functionalization of the CNT by polymers [13]. Recently, nanocomposite films were prepared from CNTs that were functionalized with poly(vinyl alcohol) (PVA) to make them dispersible in water [14]. The PVA-functionalized CNTs were then dispersed in an aqueous PVA solution and cast to create a nanocomposite film with a PVAmatrix. This approach does not require emulsifiers or surfactants to disperse the CNTs. However,

*Correspondence to:* Önder Yargı; e-mail: yargi78@gmail.com
DOI 10.1002/pc.22725
Published online in Wiley Online Library (wileyonlinelibrary.com).

the final nanocomposite film is water-soluble, of course, and of limited applicability as a protective coating. Within the past few years, it has been realized that the processing of latex dispersions offers an opportunity for blending CNTs with polymers at the nanometer scale to achieve a good dispersion in a coating matrix that is not water-soluble. The key challenge in the processing of waterborne nanocomposite coatings is to achieve the low percolation thresholds of CNTs that are predicted by theory [15]. In one of the first such reports [16], a styrene-butyl acrylate latex was blended with multi-walled CNTs that had been suspended in water using sodium dodecyl sulfate (SDS). More recently, Regev et al. [17] created nanocomposite films of poly(styrene) and poly(methyl methacrylate) using compression molding. They likewise did not functionalize the CNTs but dispersed them in water using SDS or gum Arabic. A possible drawback of this approach is that it could increase the hydrophilicity of the coating. Grunlan et al. [18] presented evidence that they had achieved a highly uniform dispersion of single-wall carbon nanotubes (SWNTs) in a poly(vinyl acetate) latex film. The SWNTs were stabilized with either GA or poly(vinyl pyrrolidone).

In the work reported here, we investigated the film formation behavior of polymer/CNTs depending on CNTs content using fluorescence technique. In this study, MWNTs were chosen, since MWNT is less expensive than SWNT, and polymer/MWNT composites may be more acceptable than polymer/SWNT composites in industrial application. Furthermore, MWNTs are easier to be dispersed in polymer matrix compared with SWNTs. Polystyrene (PS) was used as the polymer matrix because its properties are well known; it is easy to process, it is soluble in a broad range of solvents and its clarity allows dispersion of MWNTs to be optically observed at the micron scale. Films were prepared by mixing PS latex with MWNTs particles in various compositions and annealing them at temperatures above glass transition temperature of PS for 10 min intervals at temperatures ranging from 100 to 270°C. After each annealing step, fluorescence intensity, $I_p$ was monitored to observe the film formation process. The increase in $I_P/I_s$ ratio by increasing the annealing temperatures was attributed to the void-closure process. However, the decrease in $I_P/I_s$ ratio was attributed to the interdiffusion processes. $I_s$ intensity peaked at the single temperature called the void closure temperature ($T_v$).

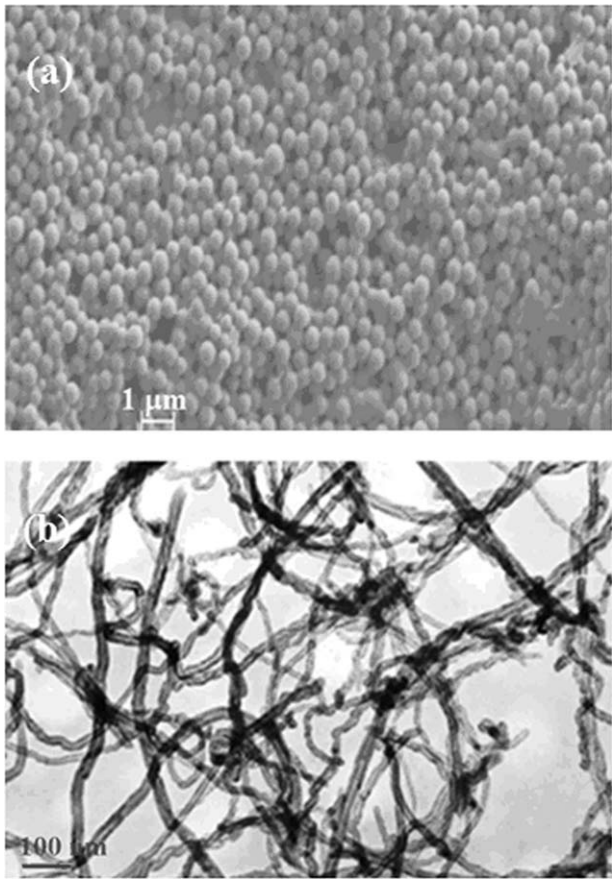


FIG. 1. (a) SEM picture of pure PS latex. (b) TEM picture of MWNT.

## EXPERIMENTAL

### *Materials*

Pyrene-labeled PS particles were produced via surfactant free emulsion polymerization process. The polymerization was performed batch-wisely using a thermostated reactor equipped with a condenser, thermocouple, mechanical stirring paddle and nitrogen inlet. The agitation rate was 400 RPM and the polymerization temperature was controlled at 70°C. Water (100 mL) and styrene (5 g) were first mixed in polymerization reactor where the temperature was kept constant (at 70°C). Potassium peroxodisulfate (KPS) initiator (0.1 g) dissolved in small amount of water (2 mL) was then introduced in order to induce styrene polymerization. Styrene monomer was first introduced in the reactor containing boiled and deionized water and then the fluorescent monomer 1-pyrenylmethyl methacrylate (PolyFluor$^{TM}$394) was dissolved in a small amount of styrene. The polymerization was conducted during 18 h. The polymer has a high glass transition temperature ($T_g = 105$°C). The latex dispersion has an average particle size of 400 nm. Figure 1a shows SEM image of PS latex produced for this study.

Commercially available MWNTs (Cheap Tubes, VT, 10–30 $\mu$m long, average inner diameter 5–10 nm, outer diameter 20–30 nm, the density is approximately 2.1 g/cm$^3$ and purity higher than 95 wt%) were used as supplied in black powder form without further purification. A stock solution of MWNTs was prepared following the manufacturers regulations: nanotubes were dispersed in deionized (DI) water with the aid of Polyvinyl Pyrrolidone (PVP) in the proportions of 10 parts MWNTs; 1–2 parts PVP; 2.000 parts DI water by bath sonication for 3


DOI 10.1002/pc

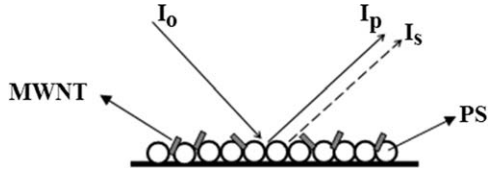


FIG. 2. Schematic illustration of sample position and incident light ($I_0$), scattered light ($I_s$), P emission ($I_P$) intensities.

h. PVP is a good stabilizing agent for dispersions of carbon nanotubes, enabling preparation of polystyrene composites from dispersions of MWNT in polystyrene solution. Figure 1b shows the TEM image of MWNTs used in this study (Cheap Tubes, VT). As seen from the Fig. 1b, the shape of MWNT is long and cylindrical.

*Preparation of PS/MWNT Composite Films*

A 15 g/L polystyrene (PS) latex in water was prepared separately. The dispersion of MWNT in water was mixed with the solution of PS yielding the required ratio, $R$ of MWNT in PS latex by using the relation:

$$R = \frac{M_{\mathrm{MWNT}}}{M_{\mathrm{PS}} + M_{\mathrm{MWNT}}} \quad (1)$$

where $M_{\mathrm{PS}}$ and $M_{\mathrm{MWNT}}$ present the weight of PS and MWNTs in the mixture, respectively. Eight different mixtures were prepared with 0, 1.5, 3, 5, 10, 15, 18, and 20 wt% MWNT by using this relation. Each mixture was stirred for 1 h followed by sonication for 30 min at room temperature. By placing the same number of drops on a glass plates with similar surface areas (0.8 × 2.5 $cm^2$) and allowing the water to evaporate at 60°C in the oven, dry films were obtained. After drying, samples were separately annealed above $T_g$ of PS for 10 min at temperatures ranging from 100 to 270°C. The temperature was maintained within ±2°C during annealing. After each annealing step, films were removed from the oven and cooled down to room temperature. The thickness of the films was determined from the weight and the density of samples and ranges from 6 to 9 μm.

*Measurements*

After annealing, each sample was placed in the solid surface accessory of a Perkin-Elmer Model LS-50

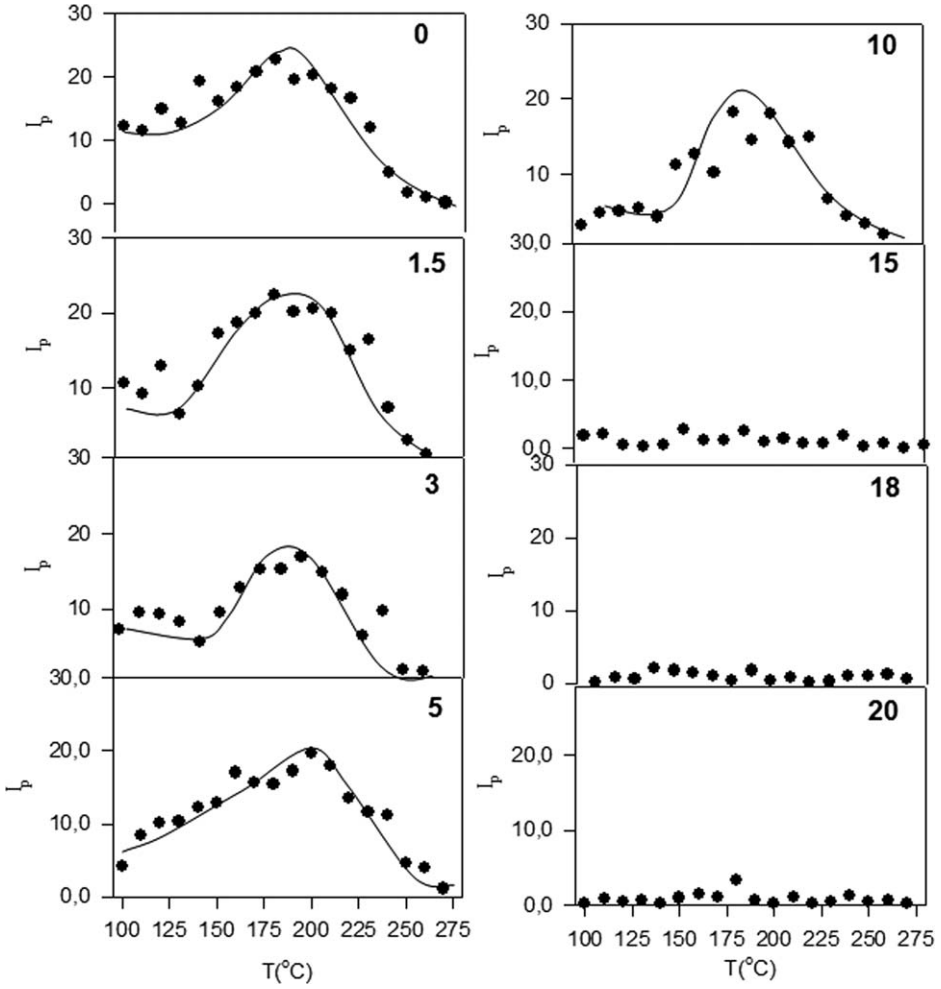


FIG. 3. Plot of ($I_P$) intensities of composite films with different MWNT content versus annealing temperatures. Numbers show MWNT content in %.

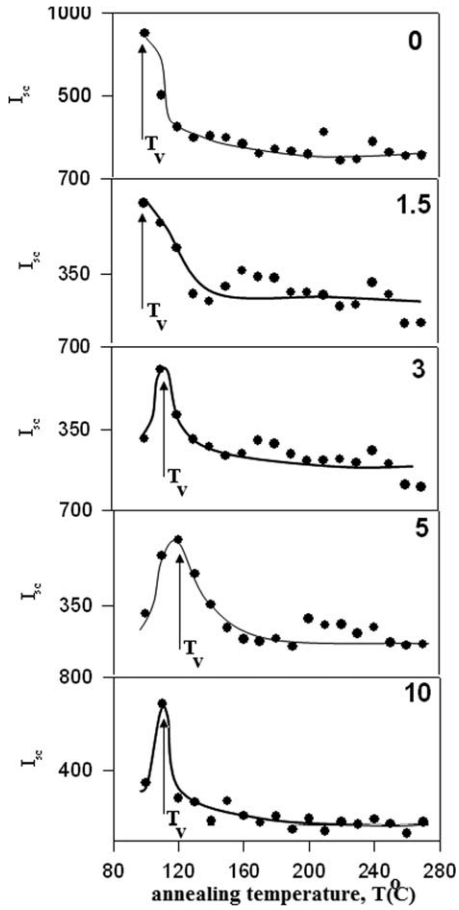


FIG. 4. Plot of ($I_{sc}$) intensities of composite films with different MWNT content versus annealing temperatures. Numbers show MWNT content in %.

fluorescence spectrometer. Pyrene (P) was excited at 345 nm and scattered light and fluorescence emission were detected between 300–500 nm. Fluorescence spectra were taken at 90° with respect to excitation light at room temperature. Slit widths were kept to provide the resolution of 8 nm during all SSF measurements. The sample position, incident ($I_o$), scattered ($I_s$) light, and emission intensity ($I_P$) are shown in Fig. 2, where it is seen that ($I_s$) is collected at right angle with respect to incident light. ***Scanning electron microscope*** (SEM) images were taken by using LEO Supra VP35 FESEM.

## RESULTS AND DISCUSSION

### *Film Formation Process of PS/MWNT Composites*

The emission and scattered intensities of the composite film with 0–20 wt% and 0–10 wt% range of MWNT content films annealed for 10 min at various temperatures are shown in Figs. 3 and 4, respectively where it is seen that both $I_P$ and $I_s$ first increase and then decrease upon annealing. $I_P/I_{sc}$ (Fig. 5) started to increase above a certain onset temperature, called the minimum film formation temperature, $T_o$ for all film samples. In Fig. 5, $T_o$ moves slightly to the higher temperature region as the MWNT content is increased. Samples above 10 wt% MWNT content show in order dispersion by indicating that fluorescence intensity is screened by MWNT particles in the composite film. Scattered light intensity, $I_s$ (Fig. 4) showed a maximum value for (0 and 1.5 wt%) and a peak for (3, 5, and 10 wt%) composites at the single temperature called void closure temperature, $T_v$. Here we have to mention that $I_s$ is scattered from the surface of the composite-film. In Fig. 3, fluorescence intensity, $I_P$ first present an increase by reaching a maximum then decreased with increasing annealing temperature. The corrected $I_P$ intensities, i.e., $I_P/I_s$ are plotted in Fig. 5 versus annealing temperature. The temperature where the $I_P/I_s$ ratio is reached to the maximum is named the healing temperature ($T_h$) as will be explained in the following section. The increase in corrected $I_P$ intensities ($I_P/I_s$) above $T_o$ presumable corresponds to the void closure process up to the $T_h$ point where healing process takes place. Decrease in corrected $I_P$ above $T_h$ can be understood by the interdiffusion processes between polymer chains at the junction surface. The behavior of corrected $I_P$ can be explained with the schematic picture in Fig. 6. In Fig. 6a, at the early stage of film formation the composite film possesses many voids, which results in short mean free, $<a>$ and optical, $s$ paths of a photon. At this stage, most of the light is scattered which yields low $I_P$. Figure 6b presents a film in which, due to the annealing, interparticle voids disappear, which give rise to a long mean free ($<a>$) and longest optical ($s$) paths. As soon as the voids are filled healing process takes place and $<a>$ and $s$ get even longer than before. At this stage, $I_P$ reaches its maximum value. Finally, Fig. 6c presents a partially transparent film with longest $<a>$ but shorter $s$ values. This film has low $I_P$ and $I_s$ intensities. This picture can be observed slightly for above the film with 10% MWNT content. For samples with higher MWNT content, the fluorescence method cannot be applied to study film formation process. Because the high opacity of the samples blocks the journey of the photon in the film and prevents fluorescence emission. The increase in $I_P/I_s$ above $T_o$ presumably corresponds to the void closure process up to the $T_h$ point where the healing process takes place. Decrease in $I_P/I_s$ above $T_h$ can be understood by interdiffusion between polymer chains.

All these results have shown that the presence of MWNT in composite film blocks and/or delays the film formation steps. In order to support these findings, SEM micrographs of composite films were taken. In Fig. 7a, for the pure PS film, no deformation in particles is observed. On the other hand, films containing 15 wt% MWNT (Fig. 7b) show a rough surface structures depending on the MWNT content in the composite film with compared to the surface of pure PS film. Due to the screening effect of MWNT, all PS particles cannot be destroyed. In order to see dispersion of MWNTs in PS lattice during annealing, SEM micrographs of composite films with 15 and 40 wt%

 DOI 10.1002/pc

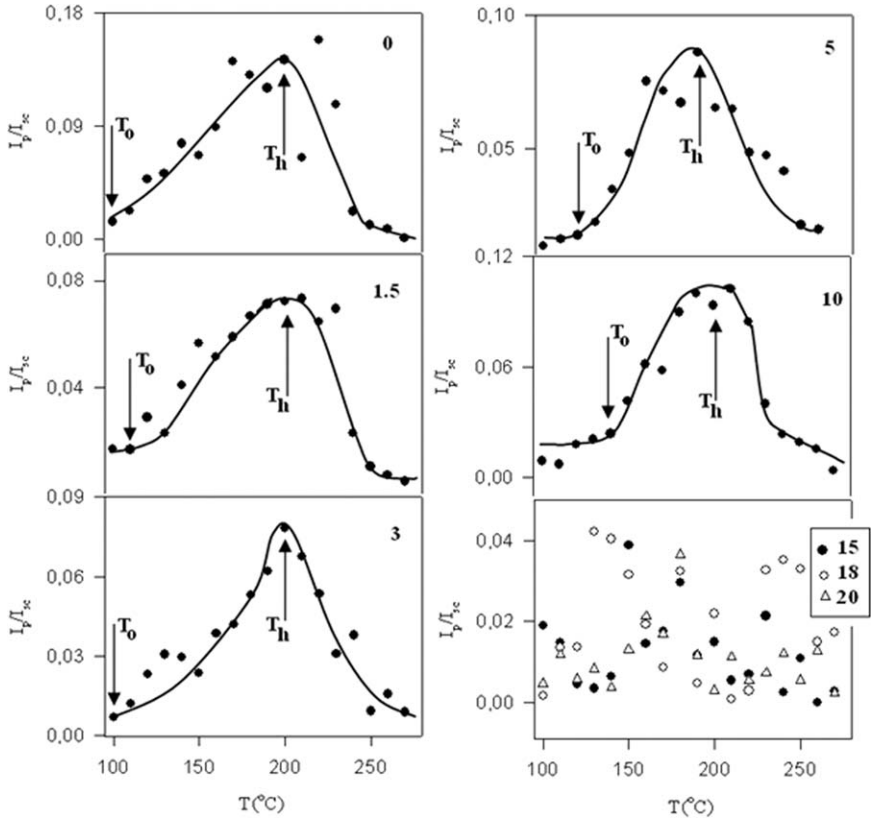


FIG. 5. Plot of corrected intensities ($I_P/I_{sc}$) of composite films with different MWNT content versus annealing temperatures. Numbers show MWNT content in %.

MWNT content in Fig. 8 also confirm this picture. Before annealing, no deformation in PS particles is observed and PS particles keep their original spherical shapes for both samples (Fig. 8a and b). After annealing treatment at 170°C, SEM images show that completes particle coalescence has been achieved (Fig. 8c and d). It can be clearly seen that the composite film consists of a network of bundles, especially in the 40 wt% MWNT content film, and indicates significant porosity. As shown in Fig. 8c carbon nanotubes are not well distributed in the polymer matrix and voids between the carbon nanoparticles and polymer matrix. The film surface is relatively even and smooth predicting that these films complete its interdiffusion processes and forms a mechanically strong continuous film. It can be clearly seen that composite film consists of a network of bundles and indicates significant porosity which results strong scattering at 170°C (Fig. 8d). This result is consistent with the microstructural analysis. The increase in $I_P/I_s$ intensity below and above $T_h$ point in the (0–10) wt% MWNT range can be explained by void closure and interdiffusion processes, respectively [19]. To understand these phenomena, the following mechanisms and their formulations are proposed.

**Voids Closure.** Latex deformation and void closure between particles can be induced by shearing stress which is generated by surface tension of polymer, i.e., polymer–air interfacial tension. The void closure kinetics can determine the time for optical transparency and latex film formation [20]. In order to relate the shrinkage of spherical void of radius ($r$) to the viscosity of surrounding medium ($\eta$) an expression was derived and given by the following relation [20].

$$\frac{dr}{dt} = -\frac{\gamma}{2\eta}\left(\frac{1}{\rho(r)}\right) \tag{2}$$

Where $\gamma$ is surface energy, $t$ is time and $\rho(r)$is the relative density. It has to be noted that here surface energy causes a decrease in void size and the term $\rho(r)$varies with the micro structural characteristics of the material, such as the number of voids, the initial particle size and packing. *Equation 2* is similar to one, which was used to explain the time dependence of the minimum film formation temperature during latex film formation [21]. If the viscosity is constant in time, integration of *Eq. 2* gives the relation as

$$t = -\frac{2\eta}{\gamma}\int_{r_0}^{r} \rho(r)dr \tag{3}$$

Where $r_0$ is the initial void radius at time $t = 0$.

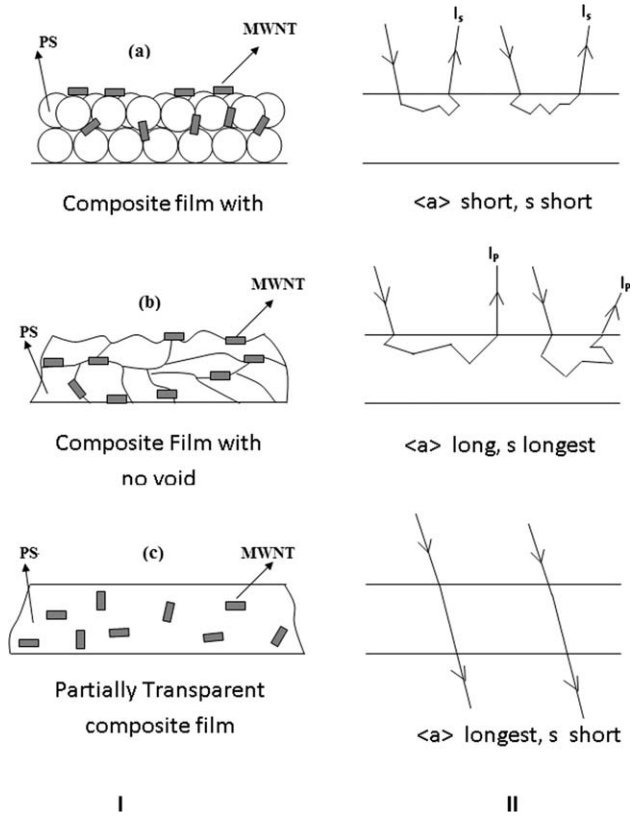


FIG. 6. Schematic illustration of the (I) composite film formation from MWNT content latex particles and (II) variation in mean free and optical paths (<*a*> and *s*) during film formation; (a), (b), and (c) correspond to the film formation stages such as (a) film in powder form, (b) film after void closure process is completed, (c) partially transparent film.

The dependence of the viscosity of polymer melt on temperature is affected by the overcoming of the forces of macromolecular interaction which enables the segments of polymer chain to jump over from one equilibration position to another. This process happens at temperatures at which free volume becomes large enough and is connected with the overcoming of the potential barrier. Frenkel-Eyring theory produces the following relation for the temperature dependence of viscosity [22–24].

$$\eta = (N_0 h/V)\exp(\Delta G/kT) \tag{4}$$

Where $N_0$ is Avogadro's number, $h$ is Planck's constant, $V$ is molar volume, and $k$ is Boltzmann constant. It is known that $\Delta G = \Delta H - T\Delta S$, then *Eq. 4* can be written as

$$\eta = A\exp(\Delta H/kT) \tag{5}$$

Where $\Delta H$ is the activation energy of viscous flow, i.e., the amount of heat which must be given to one mole of material for creating the act of a jump during viscous flow. $\Delta S$ is the entropy of activation of viscous flow. Here $A$ represents a constant for the related parameters which do not depend on temperature. Combining *Eqs. 3* and *5*, the following useful equation is obtained

$$t = -\frac{2A}{\gamma}\exp\left(\frac{\Delta H}{kT}\right)\int_{r_0}^{r}\rho(r)dr \tag{6}$$

In order to quantify the above results, *Eq. 6* can be employed by assuming that the interparticle voids are in equal size and number of voids stay constant during film formation (i.e., $\rho(r) \propto r^{-3}$), then integration of *Eq. 6* gives the relation

$$t = \frac{2AC}{\gamma}\exp\left(\frac{\Delta H}{kT}\right)\left(\frac{1}{r^2} - \frac{1}{r_0^2}\right) \tag{7}$$

Where, $C$ is a constant related to relative density $\rho(r)$.

In order to quantify the behavior of the corrected $I_P$ intensities, i.e., $I_P/I_s$ curves below $T_h$ presented in Fig. 4, void closure model can be applied, where decrease in void size ($r$) causes an increase in $I_P/(I_P)_{max}$ ratios and vice versa. If the assumption is made that $I_P/(I_P)_{max}$ ratio is inversely proportional to the sixth power of void radius, $r$ then *Eq. 7* can be written as

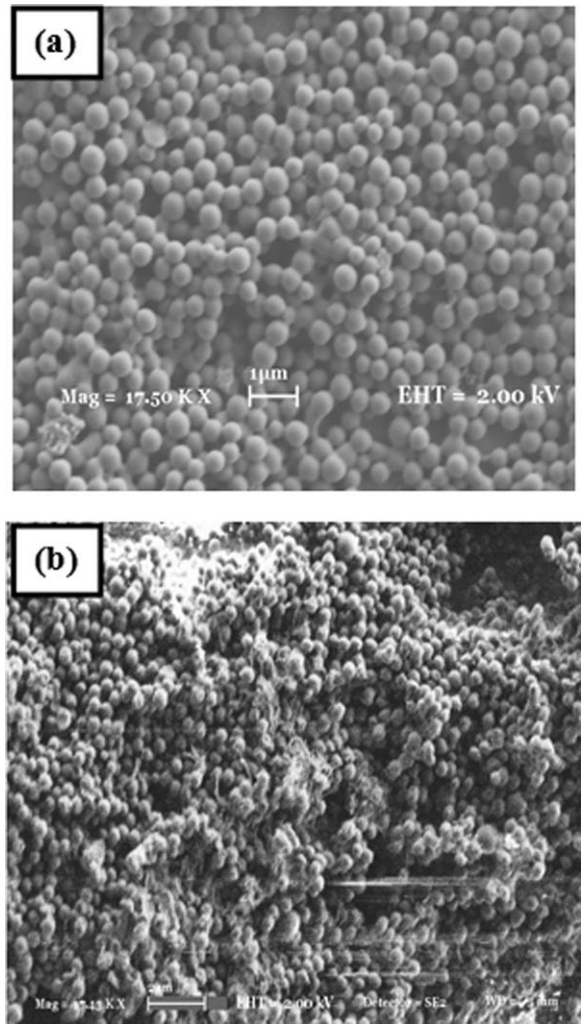


FIG. 7. (a) SEM picture of pure PS latex. (b) SEM picture of 15 wt% MWNT.


DOI 10.1002/pc

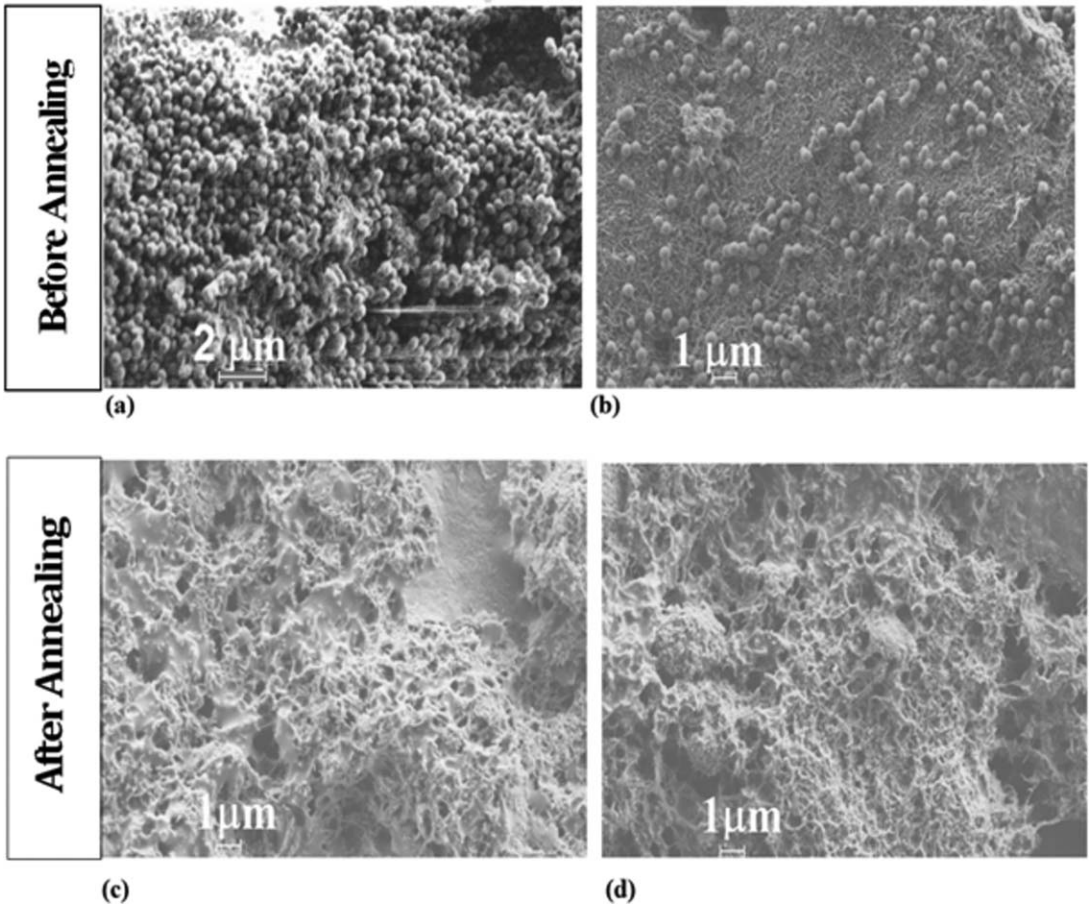


FIG. 8. SEM pictures of composite films prepared with 15 and 40 wt% MWNT content before annealing (a,b) and after annealing at 170°C (c,d), respectively.

$$t = \frac{2AC}{\gamma} \exp\left(\frac{\Delta H}{kT}\right) \left(\frac{I_P}{(I_P)_{max}}\right)^{1/3} \quad (8)$$

Here, $r_0^{-2}$ is omitted from the relation since it is very small compared to $r^{-2}$ values after a void closure process is started. *Equation 8* can be solved for $I_P/(I_P)_{max}$

$$I_P(T) = S(t) \exp\left(-\frac{3\Delta H}{kT}\right) \quad (9)$$

Where $S(t) = (\gamma t/2AC)^3$, and $I_P = I_P/(I_P)_{max}$. For a given time the logarithmic form of *Eq. 9* can be written as follows

$$\ln I_P(T) = \ln S(t) - \left(\frac{3\Delta H}{k_B T}\right) \quad (10)$$

*Equation 10* can now be used to produce viscous flow activation energies, $\Delta H$. ln $I_P$ versus $T^{-1}$ plots and their fits to *Eq. 10* are presented in Fig. 9 (right hand side of the curves) from which $\Delta H$ activation energies were obtained. The measured void closure, $\Delta H$ activation energies are listed in Table 1, which are increased, as the percent of MWNT is increased in the composite films.

**Healing and Interdiffusion.** The decrease in $I_P$ was already explained in the previous section, by the increase in transparency of latex film due to disappearing of deformed particle–particle interfaces. As the annealing temperature is increased above healing temperature ($T_h$) some part of the polymer chains may cross the junction surface and particle boundaries start to disappear, as a result $I_P$ increases due to the shorter optical and long mean free paths of a photon [19, 25–28]. In order to quantify these results, the Prager–Tirrell (PT) model [29, 30] for the chain crossing density can be employed. These authors used de Gennes's "reptation" model to explain configurational relaxation at the polymer–polymer junction where each polymer chain is considered to be confined to a tube in which executes a random back and forth motion. A homopolymer chain with N freely jointed segments of length L was considered by PT, which moves back and forth by one segment with a frequency$v$. In time, the chain displaces down the tube by a number of segments ($m$). Here, $v/2$ is called the "diffusion coefficient" of $m$ in one-dimensional motion. PT calculated the probability of the net displacement with $m$ during time $t$ in the range of $n - \Delta$ to $n - (\Delta + d\Delta)$ segments. A Gaussian probability density was obtained for small times

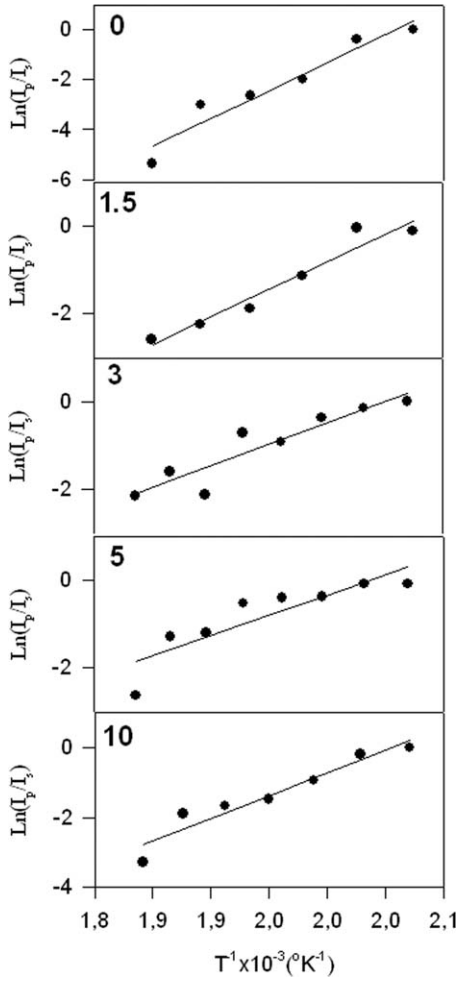


FIG. 9. Logarithmic plots of ($I_P/I_s$) data and fits to *Eq. 9* below the healing point in Fig. 5 for the 0, 1.5, 3, 5, and 10% MWNT content films annealed for 10 min.

and large $N$. The total "crossing density" $\sigma(t)$ (chains per unit area) at junction surface then was calculated from the contributions $\sigma_1(t)$ due to chains still retaining some portion of their initial tubes, plus a remainder, $\sigma_2(t)$. Here the $\sigma_2(t)$ contribution comes from chains which have relaxed at least once. In terms of reduced time $\tau=2vt/N^2$, the total crossing density can be written as

TABLE 1. Experimentally produced $d$ film thickness, activation energies.

| MWNT (%) | $d$ ($\mu$m) | $\Delta H_P$ (kcal/mol) | $\Delta E_b$ (kcal/mol) |
|---|---|---|---|
| 0.0 | 5.71 | 0.62 | 102.6 |
| 1.5 | 7.97 | 1.59 | 67.9 |
| 3.0 | 6.77 | 1.53 | 54.8 |
| 5.0 | 8.92 | 2.12 | 43.8 |
| 10.0 | 8.66 | 3.10 | 51.1 |
| 15.0 | 6.63 | – | – |
| 18.0 | 7.40 | – | – |
| 20.0 | 8.07 | – | – |

$\Delta H_P$, activation energy of void closure (measured from $I_P$); $\Delta E_b$, activation energy of backbone motion (measured from $I_P$).

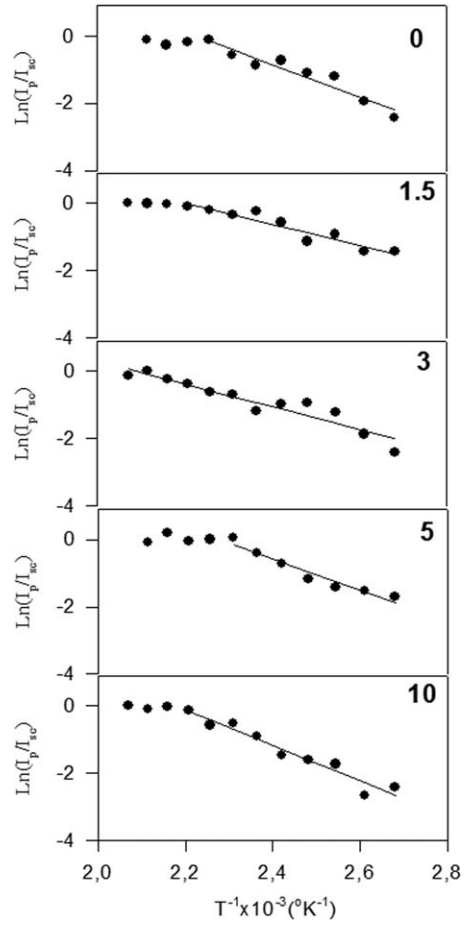


FIG. 10. The plots of (a) minimum film formation ($T_0$), (b) void closure ($T_v$), and (c) healing ($T_h$) versus MWNT content.

$$\sigma(\tau)/\sigma(\infty)=2\pi^{-1/2}\left[\tau^{1/2}+2\sum_{k=0}^{\infty}(-1)^n[\tau^{1/2}\exp(-k^2/\tau)-\pi^{-1/2}erfc(k/\tau^{1/2})]\right] \quad (11)$$

For small $\tau$ values, the summation term of the above equation is very small and can be neglected, which then results in

$$\sigma(\tau)/\sigma(\infty)=2\pi^{-1/2}\tau^{1/2} \quad (12)$$

This was predicted by de Gennes on the basis of scaling [31]. Here it should be mentioned that the dependence on time, $t$ in *Eq. 10* goes as $t^{1/4}$ at early times of healing [31]. In order to compare our results with the crossing density of the PT model, the temperature dependence of $\sigma(\tau)/\sigma(\infty)$ can be modeled by taking into account the following Arrhenius relation for the linear diffusion coefficient

$$v=v_o\exp(-\Delta E_b/kT) \quad (13)$$

Here $\Delta E_b$ is defined as the activation energy for backbone motion depending on the temperature interval. Combining *Eqs. 12* and *13* a useful relation is obtained as


DOI 10.1002/pc

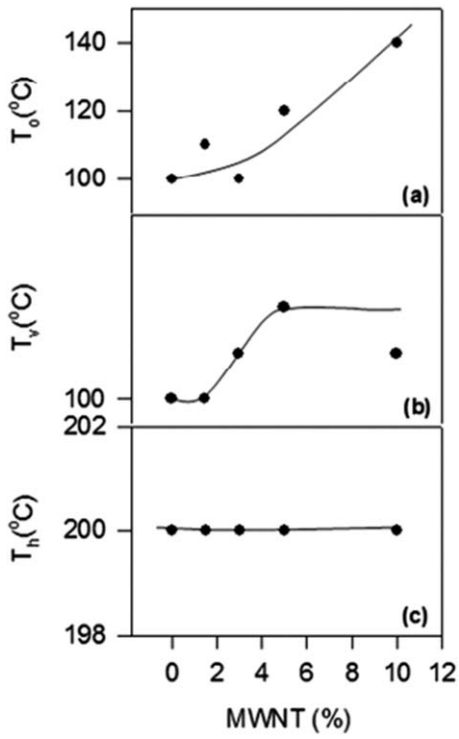


FIG. 11. The plots of (a) minimum film formation, $T_0$, (b) void closure, $T_v$ and (c) healing, $T_h$ versus MWNT content.

$$\sigma(\tau)/\sigma(\infty)=A_o\exp\left(-\Delta E_b/2kT\right) \quad (14)$$

Where $A_0=(8v_0t/\pi N^2)^{1/2}$ is a temperature independent coefficient.

The increase in $I_P/I_s$ above $T_h$ is already related to the disappearance of particle–particle interfaces, i.e., as annealing temperature is increased, more chains relaxed across the junction surface and as a result the crossing density increases. Now, it can be assumed that $I_P$ is proportional to the crossing density $\sigma(\tau)$ in *Eq. 14* and then the phenomenological equation can be written as

$$I_p(T)/I_p(\infty)=A\exp\left(-\Delta E/2kT\right) \quad (15)$$

Logarithmic plots of $I_P$ versus $T^{-1}$ are presented in Fig. 10 (left hand side of the curves) for various MWNT content. The activation energies, $\Delta E$ are produced by least squares fitting the data to *Eq. 15* and are listed in Table 1, where it is seen that $\Delta E$ values present a maximum around pure PS film (0 wt% MWNT content) while $\Delta H$ values have a minimum about the same point. It is also seen that $\Delta E_b$ values are much higher than $\Delta H_P$ Since the MWNT particles can screen the motion of polymer chain across the junction, a single chain needs more energy to overcome this difficulty. Another words interdiffusion of polymer chains needs more energy to cross over the junction surface than amount of heat which was required by one mole of polymeric material to accomplish a jump during viscous flow. Finally, minimum film formation ($T_0$), void closure ($T_v$), and healing ($T_h$) temperatures are plotted versus MWNT content in Fig. 11(a–c), where $T_0$ and $T_v$ values increase with increasing MWNT content (Fig. 11a and b). This behavior of $T_0$ and $T_v$ clearly indicates that the existence of MWNT delays the latex film formation process. However, healing processes are not affected by the presence of MWNT (Fig. 11c), which is not surprising.

## CONCLUSION

Film formation of PS/MWNT composites was investigated. It was shown that film formation from PS latex and MWNT particles can successfully be performed if the MWNT content was below 15 wt%. Below 15 wt% MWNT content, two separate stages which are named as void closure and interdiffusion were observed. In our previous study, we have investigated the film formation of PS/MLB composites [32]. It is seen that the $\Delta E_b$ values are slightly bigger than the PS/MLB system. It may be results from different of the MWNT shapes. Since MWNT distribution is long and cylindrical, screening effect of the PS/MWNT is stronger than PS/MLB system. The morphological changes were found to be consistent with the SSF results.

## REFERENCES


1. T. Provder, M.A. Winnik, and Urban M.W., Eds., Film *Formation in Waterborne* Coatings, ACS *Symposium* Series, American Chemical Society, Washington, 648 (1996).
2. P.R. Sperry, B.S. Snyder, M.L. O'Dowd, and P.M. Lesko, *Langmuir* **10**, 2619 (1994).
3. J.K. Mackenzie and R. Shuttleworth, *Proc. Phys. Soc*., **62**, 838 (1949).
4. J.L. Keddie, *Mater. Sci. Eng*., **R21**, 101 (1997).
5. J.N. Yoo, L.H. Sperling, C.J. Glinka, and A. Klein, *Macromolecules*, **24**, 2868 (1991).
6. Ö. Pekcan, *Trends Polym. Sci*., **2**, 236 (1994).
7. W.A. de Heer, *MRS Bull*. **29**, 281 (2004).
8. A.B. Dalton, S. Collins, J. Razal, E. Munoz, V.H. Ebron, and B.G. Kim, *J. Mater. Chem*., **14**, 1 (2004).
9. R. Andrews, D. Jacques, A.M. Rao, T. Rantell, and F.E. Derbyshir, *Appl. Phys. Lett*. **75**, 1329 (1999).
10. J.K.W. Sandler, J.E. Kirk, I.A. Kinloch, M.S.P. Shaffer, and A.H. Windle, *Polymer*, **44**, 5893 (2003).
11. J.K.W. Sandler, S. Pegel, M. Cadek, F. Gojny, M. van Es, and J. Lohmar, *Polymer*, **45**, 2001 (2004).
12. B.P. Grady, F. Pompeo, R.L. Shambaugh, and D.E. Resasco, *J. Phys. Chem. B*, **106**, 5852 (2002).
13. R. Sainz, A.M. Benito, M.T. Martinez, J.F. Galindo, J. Sotres, A.M. Baro, B. Corraze, O. Chauvet, A.B. Dalton, R.H. Baughma, and W.K. Maser, *Nanotechnology*, **16**, S150 (2005).
14. Y. Lin, B. Zhou, K.A.S. Fernando, P. Liu, L.F. Allard, and Y.P. Sun, *Macromolecules*, **36**, 7199 (2003).
15. M. Foygel, R.D. Morris, D. Anez, S. French, and V.L. Sobolev, *Phys. Rev. B*, **71**, 104201 (2005).
16. A. Dufresne, M. Paillet, J.L. Putaux, R. Canet, F. Carmona, P. Delhaes, and S. Cui, *J. Mater. Sci*., **37**, 3915 (2002).
17. O. Regev, P.N.B. Elkati, J. Loos, and C.E. Koning, *Adv. Mater*., **16**, 248 (2004).

18. J.C. Grunlan, A.R. Mehrabi, M.V. Bannon, and J.L. Bahr, *Adv. Mater*., **16**, 150 (2004).
19. S. Ugur, Ö. Yargi, and Ö. Pekcan, *Compos. Interface*, **15**, 411 (2008).
20. J.L. Keddie, P. Meredith, R.A.L. Jones, and A.M. Donald, "Film Formation in Waterborne Coatings," in *ACS Symposium Series*, *Vol*. 648, T. Provder, M.A. Winnik, and M.W. Urban, Eds., American Chemical Society, Washington, 332–348 (1996).
21. G.B. Mc Kenna, In *Comprehensive Polymer Science*, *Vol.* 2, C. Booth and C. Price, Eds., Pergamon Press, Oxford, UK (1989).
22. H. Vogel, *Phys. Z*., **22**, 645 (1925).
23. G.S. Fulcher, *J. Am. Ceram. Soc*., **8**, 339 (1925).
24. J. Frenkel, *J. Phys. USSR*, **9**, 385 (1945).
25. O. Pekcan and E. Arda, *Encyclopedia of Surface and Colloid Science*, Marcel and Dekker, New York, 2691 (2002).
26. O. Pekcan, E. Arda, V. Bulmus, and E. Piskin, *J. Appl. Polym. Sci*., **77**, 866 (2000).
27. E. Arda, F. Ozer, E. Piskin, and O. Pekcan, *J. Coll. Interface Sci*., **233**, 271 (2001).
28. E. Arda and Ö. Pekcan, *Polymer*, **42**, 7419 (2001).
29. S. Prager and M. Tirrell, *J. Chem. Phys*., **75**, 5194 (1981).
30. R.P. Wool, B.L. Yuan, and O.J. McGarel, *J. Polym. Eng. Sci*., **29**, 1340 (1989).
31. P.G. de Gennes, *J. Chem. Phys*., **76**, 3322 (1982).
32. Ş. Uğur, Ö.Yargı, E. Günister, and Ö. Pekcan, *Appl. Clay Sci*., **42**, 39 (2008).

 DOI 10.1002/pc